

ARTICLE

Theoretical Insight into the Redox-switchable Activity of Group 4 Metal Complexes for the Ring-Opening Polymerization of ϵ -Caprolactone

Received 00th January 20xx,
Accepted 00th January 20xx

DOI: 10.1039/x0xx00000x

Xiaowei Xu,^a Gen Luo,^{*,a} Zhaomin Hou,^b Paula L. Diaconescu,^{*,c} and Yi Luo^{*,a}

Redox-switchable polymerization has drawn increasing attention, in particular for the ring-opening polymerization (ROP) of biomass-derived monomers. However, an understanding of how the switch determines the observed changes is still limited. In this study, DFT calculations were employed to understand the redox-switchable ROP mechanism of ϵ -caprolactone catalyzed by group 4 metal complexes bearing [OSSO]-type ferrocene ligands. Our results suggest that two oxidized forms show higher reactivity because of the higher Lewis acidity of their catalytic metal centers in comparison with that of the corresponding reduced states. In one case, however, a lower activity of the oxidized species was observed that is likely due to the increased stability of the substrate-catalyst intermediate leading to a high activation barrier. In addition, other analogous metal complexes were computationally modelled by changing the metal center or modifying the ancillary ligand with different bridging-heteroatoms, and the results provide useful information on the development of new redox-switchable polymerization catalysts.

Introduction

Polyesters are attractive materials due to their biodegradability and biocompatibility, and have been applied in the packaging or textile industry and biomedicine.¹ Therefore, the development of efficient strategies for the synthesis of such polymers is of great significance. In this context, the ring-opening polymerization (ROP) of cyclic esters catalyzed by single-site metal alkoxides is an efficient approach.² In particular, the redox-switchable ROP of cyclic esters has drawn an increasing attention in the last decade since it can regulate the (co)polymerization process and thus the resulting polymer microstructure.³ In 2006, Long and Gibson first applied the redox-switchable strategy to the ROP of *rac*-lactide (LA) catalyzed by a titanium bis(iminophenoxide)(salen) complex bearing two ferrocenyl (Fc) units via altering the oxidation state of the ferrocene iron center.⁴ Since then, several catalysts have been developed by either modulating the oxidation state of the central metal⁵ or that of the supporting ligand.⁶ For example, Byers and coworkers demonstrated that Fe(II) bis(imino)pyridine complexes were superior catalysts compared

to Fe(II)/Fe(III) analogues for the ROP of ϵ -caprolactone (CL).^{5a} They further computationally investigated the role of the alkoxide initiator and the electronic structures of these redox-active iron species.⁷ Their results suggested that the coordination of the lactone monomer is a key factor accounting for the reactivity trend. The redox non-innocence of the bis(imino)pyridine ligand allows access to a masked low-coordinate monoalkoxide Fe(II) center, which facilitates binding considerably relative to a similar bisalkoxide Fe(II) complex.

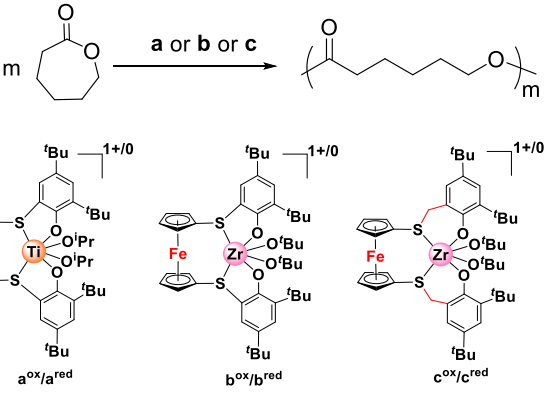
Furthermore, Diaconescu and co-workers^{6b} demonstrated that an aluminum complex bearing an [OSSO]-type bis(phenolato) ferrocene ligand, (thiolfan*)Al(O^tBu) (thiolfan* = 1,1'-di(2,4-di-*tert*-butyl-6-thiophenoxy)ferrocene), could catalyze CL/LA (co)polymerization. DFT calculations in that work suggested that the coordination of the carbonyl group of the pre-enchained monomer unit accounted for the propagation rate of such (co)polymerizations. In addition, a series of titanium and zirconium alkoxide complexes bearing similar ferrocene ligands, (thiolfan*)Ti(OⁱPr)₂, (thiolfan*)Zr(O^tBu)₂, and (thiolfan)Zr(O^tBu)₂ (thiolfan = (1,1'-di(2,4-di-*tert*-butyl-6-thiomethylenephenoxy)ferrocene), Table 1) were used for CL polymerization.^{6a,f} As shown in Table 1, although the three couples of group 4 metal complexes (**a**^{ox}/**a**^{red}, **b**^{ox}/**b**^{red}, and **c**^{ox}/**c**^{red}) have a similar ancillary ligand framework, their oxidized and reduced forms demonstrated significantly diverse redox-switchable performance in CL polymerization. For instance, the oxidized forms **a**^{ox} and **c**^{ox} showed a higher activity toward CL polymerization compared with the corresponding reduced forms, **a**^{red} and **c**^{red}. However, the **b** system showed a reverse redox-switchable behavior (Table 1).

^a State Key Laboratory of Fine Chemicals, School of Chemical Engineering, Dalian University of Technology, Dalian 116024, China. E-mail: luogen@dlut.edu.cn, luoyi@dlut.edu.cn

^b Organometallic Chemistry Laboratory, RIKEN Cluster for Pioneering Research, and Advanced Catalysis Research Group, RIKEN Center for Sustainable Resource Science, 2-1 Hirosawa, Wako, Saitama 351-0198, Japan.

^c Department of Chemistry and Biochemistry, University of California, Los Angeles, 607 Charles E. Young Drive East, Los Angeles, California 90095, United States. Email: pld@chem.ucla.edu

Electronic Supplementary Information (ESI) available: [details of any supplementary information available should be included here]. See DOI: 10.1039/x0xx00000x

Table 1. Group 4 metal catalysts bearing [OSSO]-type bis(phenolato) ferrocene-based ligands for ϵ -caprolactone (CL) polymerization.^{6a,6f}


entry ^a	compound ^a	Temp (°C)	Time (h)	Conv. (%)
1	a^{ox}	100	4	48
2	a^{red}	100	2	<5
3	b^{ox}	50	20	84
4	b^{red}	50	8	89
5	c^{ox}	100	1.5	97
6	c^{red}	100	1.5	52

^a The right superscripts "ox" and "red" denote oxidized and reduced states, respectively.

These intriguing reactions indicate that the redox-switchable activity of such catalysts is strongly dependent on their supporting ligands and catalytic metal centers and, therefore, are an appropriate choice to study computationally.^{8,9} The elucidation of the origin of the redox-switchable performance is not only of interest but also of importance for the further development of redox-switchable polymerization catalysts. In the present work, the mechanism of redox-switchable ROP of CL catalyzed by **a**, **b**, **c** (Table 1) is studied by DFT calculations. In addition, some potential group 4 metal analogues with a high performance for the redox-switchable ROP of CL are proposed on the basis of computational studies.

Computational details

The B3PW91 functional¹⁰ corrected with the empirical dispersion term (known as Grimme-D3 with the zero-damping scheme)¹¹ was used for geometrical optimizations and subsequent frequency calculations without any symmetry or geometrical constraints. In these calculations, the 6-31G(d) basis set¹² was used for non-metallic atoms, while the Ti, Zr, and Hf atoms were treated by the Stuttgart/Dresden effective core potential (ECP)¹³ together with the associated basis sets. Such basis sets are referred to as BSI. To obtain accurate energies, single-point energy calculations were performed for the optimized geometries at the level of M06¹⁴/BSII together with the CPCM model¹⁵ (in benzene solution) to consider the solvation effect. In the BSII, the Stuttgart/Dresden ECP and associated basis sets were used for metal atoms, and the 6-311G(d,p) was used for the remaining atoms. The right-superscripts "ox" and "red" of a given label (e.g., **a^{ox}** or **a^{red}**)

denote the oxidized or reduced forms of the corresponding complex, respectively. The profiles of free energy in solution reported in this study were obtained at the M06/BSII (CPCM, benzene)//B3PW91-D3/BSI level, including the free energy correction taken from gas-phase frequency calculations. The corresponding relative enthalpies (ΔH , kcal mol⁻¹) are also provided for the estimation of entropy effects. All calculations were carried out by using the Gaussian 16 program package.¹⁶ For the sake of computational efficiency, the O^tBu and OⁱPr groups were replaced by OMe groups. The computational model adopted here was successfully applied for similar systems in previous studies.^{6b,c} The three-dimensional images of the optimized structures were prepared using CYLview.¹⁷

Results and discussion

Comparison of the active species

Before discussing the redox-switchable mechanism, the geometric and electronic characteristics of the oxidized and reduced species of **a**, **b**, and **c** were analysed. The computational results show that the doublet and singlet are the most stable states of the oxidized and reduced species, respectively, for each of the three cases. As shown in Fig. 1, each oxidized species has a similar geometric structure to the corresponding reduced form. The metal–S distances in the oxidized forms are slightly longer than those in the reduced forms, suggesting a partial oxidation of the metal–S bonds. Electronically, the catalytic metal centre has a more positive charge in the oxidized than that in the reduced species. It is also noted that the Zr centres in **b** and **c** are more positively charged compared with Ti in **a**, in line with the stronger acidity of the former than of the latter. In all cases, the ferrocene iron centres have a lower positive charge than the group 4 metals.

In addition, our DFT calculations indicate that the singly occupied molecular orbitals (SOMO) of the three oxidized active species (**a^{ox}**, **b^{ox}**, and **c^{ox}**) and the spin densities are mainly localized on the ferrocene fragment (Figs 1 and S1), suggesting that the one-electron oxidation is a ferrocene-based process.

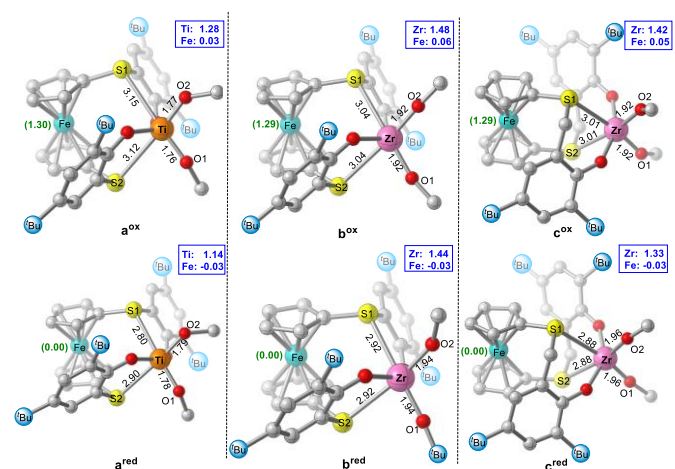


Fig. 1 Optimized structures (distances in Å) of pre-catalysts. All hydrogen atoms were omitted for clarity. The Mulliken charges on metal atoms are given in blue. The data in green given in parenthesis denote the spin density at the iron centers.

ARTICLE

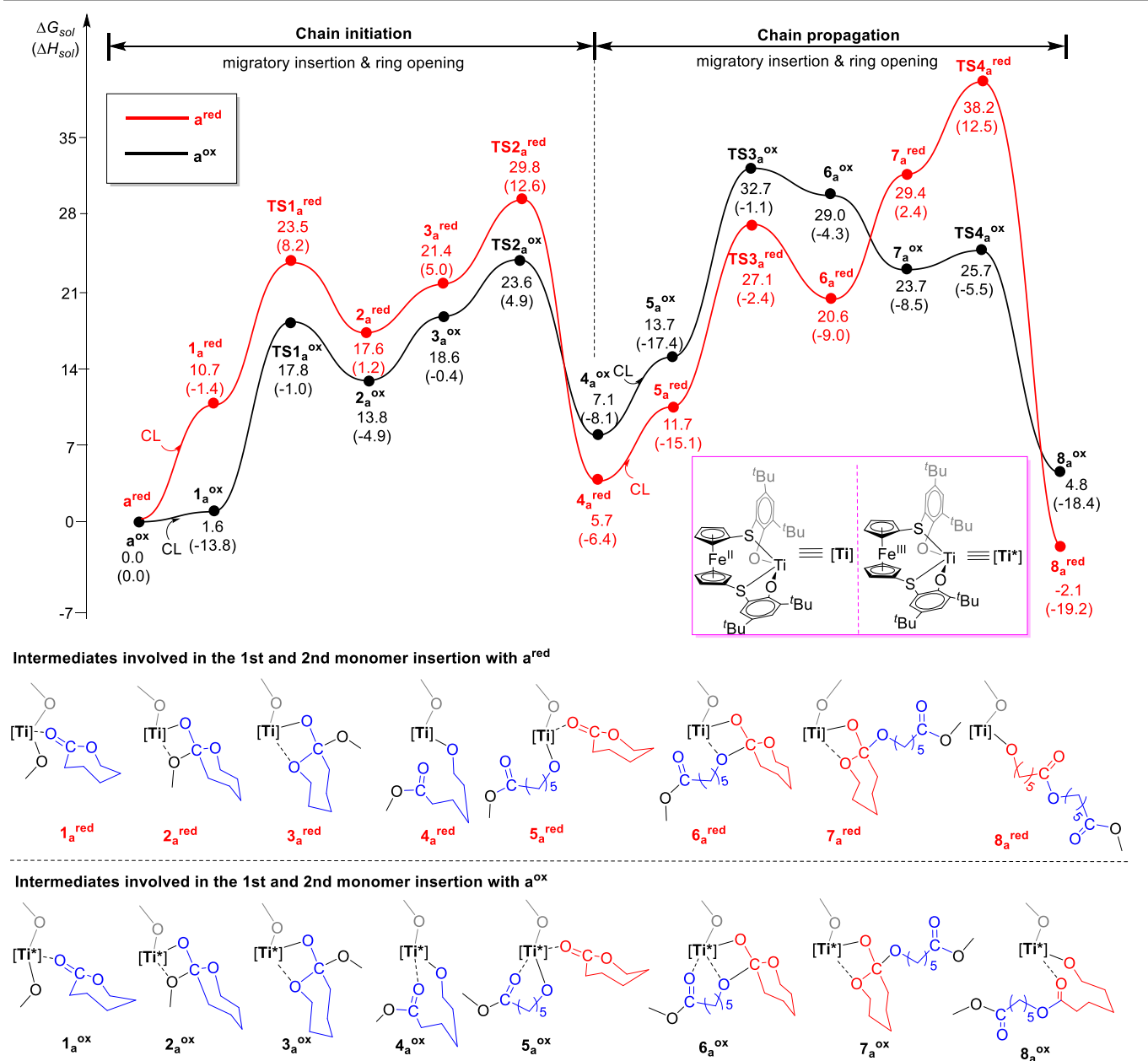


Fig. 2 Energy profiles of the chain initiation and propagation steps catalyzed by a^{ox} and a^{red} . The relative free energy and enthalpy values (in parentheses) are given in kcal mol⁻¹.

However, we note that the similar one-electron redox process of some ferrocene-containing bi- or multi-nuclear metal complexes did not occur at iron.^{18,19} Nonetheless, the results discussed herein still apply.¹⁸

ROP of CL Catalyzed by a^{ox}/a^{red}

The metal complex catalyzed ROP of cyclic esters such as CL usually follows a coordination-insertion mechanism, which includes a migratory insertion of the alkoxide group and

subsequent ring-opening events.^{2d,g,20} Taking this mechanism into account, the chain initiation and propagation steps of CL polymerization catalyzed by **a** (both the oxidized **a^{ox}** and reduced **a^{red}** species) were calculated. As shown in Fig. 2, the **a^{ox}**-catalyzed CL polymerization starts with the formation of **1_{a^{ox}}**, which is endergonic by 1.6 kcal mol⁻¹. Then, the migratory insertion of the OMe group into the C=O bond of CL takes place via a transition state (TS), **TS1_{a^{ox}}**, with an energy barrier of 17.8 kcal mol⁻¹, leading to the intermediate **2_{a^{ox}}**. Prior to ring-opening, an isomerization of **2_{a^{ox}}** to **3_{a^{ox}}** occurs, during which the Ti...OMe interaction disappears and a new bonding interaction is formed instead between titanium and the ring oxygen atom of the CL unit. Attempts to locate such an isomerization TS were fruitless. However, a relaxed potential energy surface scan indicated that an electronic energy of 7.7 kcal mol⁻¹ seems to be required to achieve the isomerization of **2_{a^{ox}}** to **3_{a^{ox}}** (Fig. S2). Such an energy is lower than that for the ring-opening TS (electronic energy of 7.7 vs 12.3 kcal mol⁻¹ relative to **2_{a^{ox}}**). Similar results were found for the reduced case (4.2 vs 14.4 kcal mol⁻¹ for the electronic versus the activation energy, respectively). These data suggest that such an isomerization event could not be turnover limiting. The subsequent ring-opening goes through the transition state **TS2_{a^{ox}}** with an energy barrier of 23.6 kcal mol⁻¹, which is 5.8 kcal mol⁻¹ higher than that for the migratory insertion step (**TS1_{a^{ox}}**). The resulting ring-opening product **4_{a^{ox}}** shows a strong chelation interaction between the carbonyl oxygen and the catalytic center ($d_{\text{Ti-O3}} = 2.37 \text{ \AA}$, Fig. 3). The whole process of the ring-opening of the first CL is endergonic by 7.1 kcal mol⁻¹.

At the chain propagation stage, similarly to during chain initiation, the carbonyl oxygen of CL coordinates to the Ti center in **4_{a^{ox}}**, forming **5_{a^{ox}}**. The intermediate **5_{a^{ox}}** has a higher free energy than **1_{a^{ox}}** by 12.1 kcal mol⁻¹ possibly due to a relatively coordinative saturation in the former. The subsequent migratory insertion needs to overcome a high energy barrier of 32.7 kcal mol⁻¹ through **TS3_{a^{ox}}**, yielding the intermediate **6_{a^{ox}}** and, further, **7_{a^{ox}}** via isomerization. The subsequent ring opening easily takes place through **TS4_{a^{ox}}** to give the product **8_{a^{ox}}**. Taken together, the CL polymerization catalyzed by **a^{ox}** has an overall activation barrier of 32.7 kcal mol⁻¹, which could be

kinetically accessible under the experimental conditions (100 °C). We note that although the reaction is endergonic for the first CL monomer ring opening, the reaction with the second CL implantation is actually exergonic by 2.3 kcal mol⁻¹ (the energy of **8_{a^{ox}}** relative to **4_{a^{ox}}**). In this sense, it would eventually be an exergonic process with the growth of the polymer chain.

In the case of the reduced form **a^{red}**, the CL polymerization goes through a similar pathway as the oxidized species (Fig. 2). Notably, in **4_{a^{red}}** and **8_{a^{red}}**, there is no additional Ti...O chelation interaction between Ti and the carbonyl in the pre-enriched CL unit, in contrast to the corresponding oxidized species **4_{a^{ox}}** and **8_{a^{ox}}** (Fig. 3). In addition, it was found that the ring-opening step of the second CL via **TS4_{a^{red}}** has a higher energy barrier (38.2 kcal mol⁻¹) than that for migratory insertion via **TS3_{a^{red}}** (27.1 kcal mol⁻¹) and thus serves as the turnover-limiting step of the polymerization catalyzed by the reduced species. Such a high energy barrier makes the reduced form **a^{red}** unable to promote the chain propagation, in line with the experimentally observed difference between **a^{ox}** and **a^{red}**.^{6f}

It is important to note that, at the chain initiation stage, the reduced species **a^{red}** is less active than **a^{ox}**, as suggested by the corresponding energy barriers (38.2 versus 32.7 kcal mol⁻¹ overall activation barrier, Fig. 2). In order to understand this difference further, a distortion/interaction analysis²¹ was performed for the transition states **TS1_{a^{ox}}** and **TS1_{a^{red}}**. The transition states were decomposed into two fragments, the monomer moiety (fragment B) and the remaining metal complex (fragment A), and their energies were evaluated through single-point calculations. The single-point energies of the fragments and the energy of the transition state were used to estimate the interaction energy, ΔE_{int} . These single-point energies, together with the energies of the respective fragments in their optimal geometry, allow the estimation of the deformation energies of the two fragments, $\Delta E_{\text{def}}(\text{A})$ and $\Delta E_{\text{def}}(\text{B})$. The deformation energy of a fragment is defined as the energy difference between its distorted geometry in the transition state and its optimized structure. Therefore, the energy of the transition state, ΔE_{TS} , is $\Delta E_{\text{TS}} = \Delta E_{\text{int}} + \Delta E_{\text{def}}(\text{A}) + \Delta E_{\text{def}}(\text{B})$.

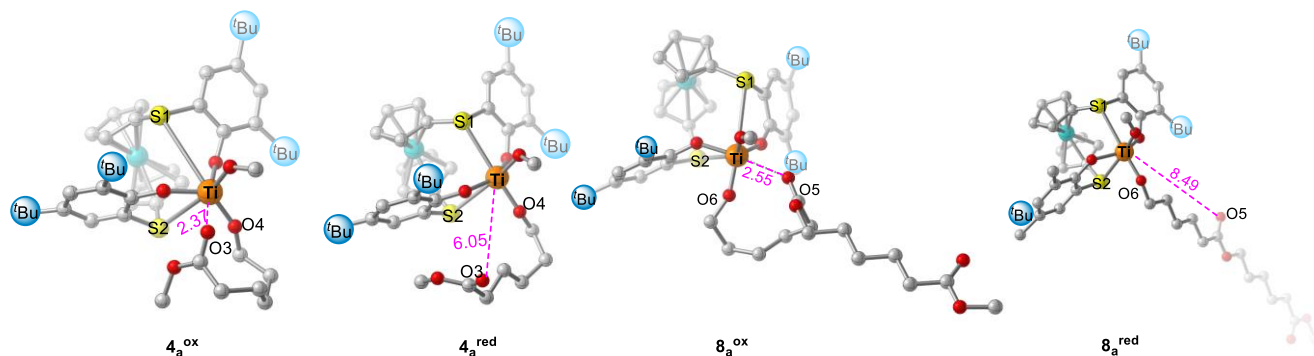


Fig. 3 Optimized structures (distances in Å) of the insertion and ring-opening products of the first and second monomers for the reaction of CL with **a^{ox}** and **a^{red}**

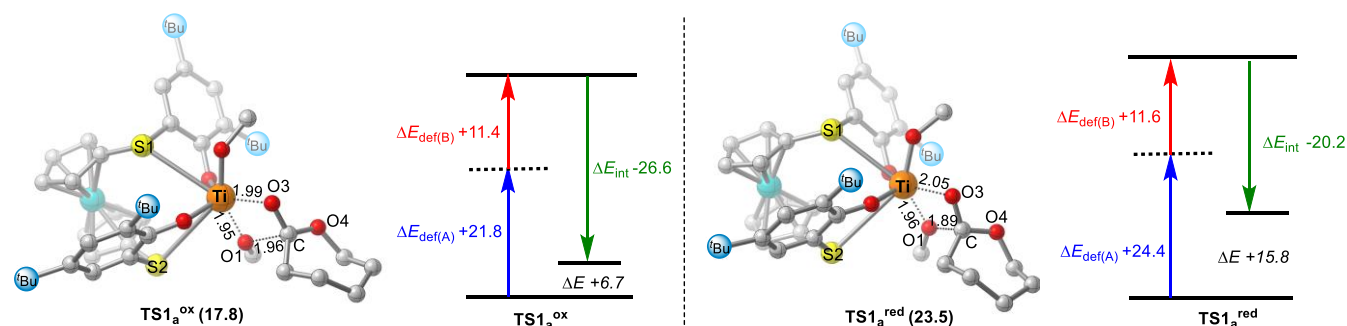


Fig. 4 Optimized structures (distances in Å) and distortion/interaction analysis of **TS1_a^{ox}** and **TS1_a^{red}**. Values in parentheses are the relative Gibbs free energy barriers. Energies are given in kcal mol⁻¹.

As shown in Fig. 4, the interaction energies ΔE_{int} between the catalyst fragment and CL moiety in **TS1_a^{ox}** (−26.6 kcal mol⁻¹) and **TS1_a^{red}** (−20.2 kcal mol⁻¹) could partly offset the unfavorable total deformation energy ΔE_{def} (33.2 for **oxTS1_a**, 36.0 kcal mol⁻¹ for **TS1_a^{red}**). Overall, the ΔE_{TS} value of **TS1_a^{ox}** is smaller than that of **TS1_a^{red}** by 9.1 kcal mol⁻¹. Therefore, the stronger interaction between the two fragments accounts for the lower energy of **TS1_a^{ox}** than that of **TS1_a^{red}**. It is noteworthy that, during the chain propagation, the intermediates **4_a**, **5_a**, and **6_a** in their oxidized forms have higher relative free energies than the corresponding reduced species (Fig. 2). This phenomenon is different from that in the chain initiation. This is possibly due to different enthalpy effects as suggested by the corresponding enthalpy values (Fig. 2), where the oxidized forms of **4_a**, **5_a**, and **6_a** are lower in enthalpy compared with their reduced forms, being similar to that in the chain initiation step. As to the higher relative free energy of **TS3_a^{ox}** than of **TS3_a^{red}**, it is possible that the coordination of the carbonyl of the pre-enchained CL unit makes titanium more crowded; in turn, this weakens the interaction between titanium and an incoming CL monomer and further destabilizes **TS3_a^{ox}** (Fig. S3). This is different from what was observed for the aluminum complex supported by the same ligand,^{6b} where the propagation step was facilitated by the chelation effect in the oxidized state.

As mentioned above, the ring-opening step of the propagation stage, **TS4_a^{red}** has a significantly higher relative energy than **TS4_a^{ox}** (38.2 vs 25.7 kcal mol⁻¹, Fig. 2). A closer analysis of the structures of these two transition states could provide further information to understand such an energy difference. As shown in Fig. 5, the Ti-O6 and Ti-O5 distances in **TS4_a^{ox}** are shorter than the corresponding values in **TS4_a^{red}** (2.01 vs 2.09 Å, 1.96 vs 1.97 Å, respectively), suggesting a stronger interaction between titanium and the growing chain in the oxidized species. This result is similar to that observed for the initiation step (**TS2_a^{ox}** and **TS2_a^{red}**, Fig. 5). Therefore, the stronger interaction between the metal center and the growing chain (or incoming monomer) is likely responsible for the higher reactivity of the oxidized than the reduced species, as experimentally observed. Such a stronger interaction in the oxidized forms could be reasonably attributed to the stronger Lewis acidity of the titanium center, as manifested by the higher positive charges in comparison with those of the reduced forms (Fig. S4). This situation is different from the redox-switchable

polymerization of trimethylene carbonate by an indium complex, where the ferrocene-oxidation induced elongation of In–N distances rather than the Lewis acidity of the metal center allowed a stronger monomer binding.⁹

ROP of CL Catalyzed by **b^{ox}**/**b^{red}**

As aforementioned, the Zr complexes **b^{ox}** and **b^{red}** showed a dramatically different activity compared with their Ti analogues (**a^{ox}**/**a^{red}**).^{6a,f} Unlike **a^{ox}**/**a^{red}**, **1_b^{red}** was more active than **1_b^{ox}** toward CL polymerization.^{6a} To have a better understanding of such an experimental observation, the energy profiles of CL polymerization mediated by **b^{ox}** and **b^{red}** were investigated. As shown in Fig. 6, the initial monomer coordination in **1_b^{ox}** is more stable than the isolated **b^{ox}** and CL monomer by 5.5 kcal mol⁻¹, while its reduced analogue **1_b^{red}** is higher in energy than the reactants by 5.6 kcal mol⁻¹. In the case of the oxidized species, **1_b^{ox}** subsequently undergoes the migratory insertion (**TS1_b^{ox}**) and ring opening (**TS2_b^{ox}**) by overcoming energy barriers of 17.8 and 20.7 kcal mol⁻¹, respectively, yielding the intermediate **4_b^{ox}** with a carbonyl chelation interaction ($d_{\text{Zr} \cdots \text{O}3} = 2.34$ Å, Fig. S5). During chain propagation, the coordination of CL to **4_b^{ox}** is exergonic by 4.3 kcal mol⁻¹, similar to the chain initiation step. Then, a migratory insertion occurs via **TS3_b^{ox}** with an energy barrier of 23.0 kcal mol⁻¹ (**1_b^{ox}** → **TS3_b^{ox}**), yielding **6_b^{ox}**. After an isomerization of **6_b^{ox}** to **7_b^{ox}**, the ring opening reaction takes place to give the product **8_b^{ox}**. The overall free energy barrier of the **1_b^{ox}**-catalyzed pathway is 28.7 kcal mol⁻¹ (**TS4_b^{ox}**) relative to **1_b^{ox}**. In the case of the reduced species, although the stationary points are higher in energy than those for the corresponding oxidized species, the overall energy barrier is only 25.1 kcal mol⁻¹ (**TS4_b^{red}**), which is lower than that for the reaction profile involving the oxidized species (28.7 kcal mol⁻¹). This result suggests that the activity of **b^{red}** is higher than that of **b^{ox}**, in agreement with the experimentally observed reactivity difference between the two oxidation states.^{6a} A comparison of the two pathways (Fig. 6) indicates that the higher energy barrier for the oxidized species is caused by the higher stability of **1_b^{ox}** and **5_b^{ox}** than of **b^{ox}**. In view of the shorter Zr...O(carbonyl) distance in **1_b^{ox}** than in **1_b^{red}** (2.33 vs 2.40 Å, Fig. S6), this stability may be originated from a stronger binding between the metal center and the coordinating monomer.

ARTICLE

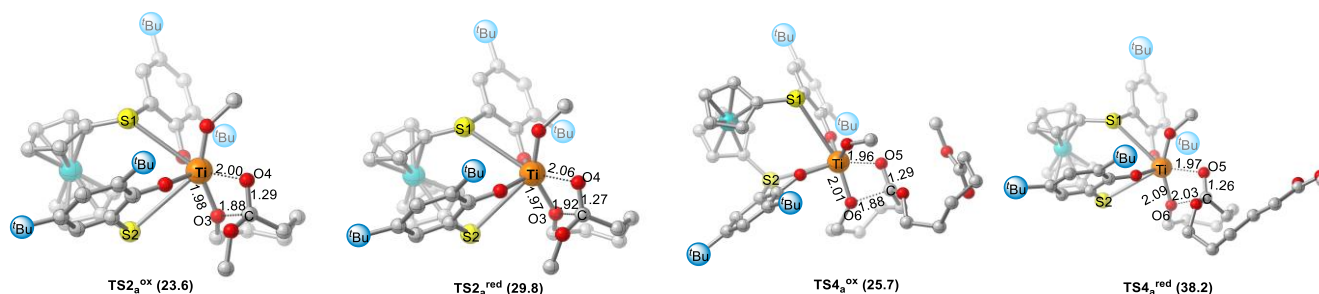


Fig. 5 Optimized structures (distances in Å) and energies of the transition states (TS2_a^{ox} vs TS2_a^{red}, TS4_a^{ox} vs TS4_a^{red}). Values in parentheses are the free energies relative to isolated reactants. Energies are given in kcal mol⁻¹.

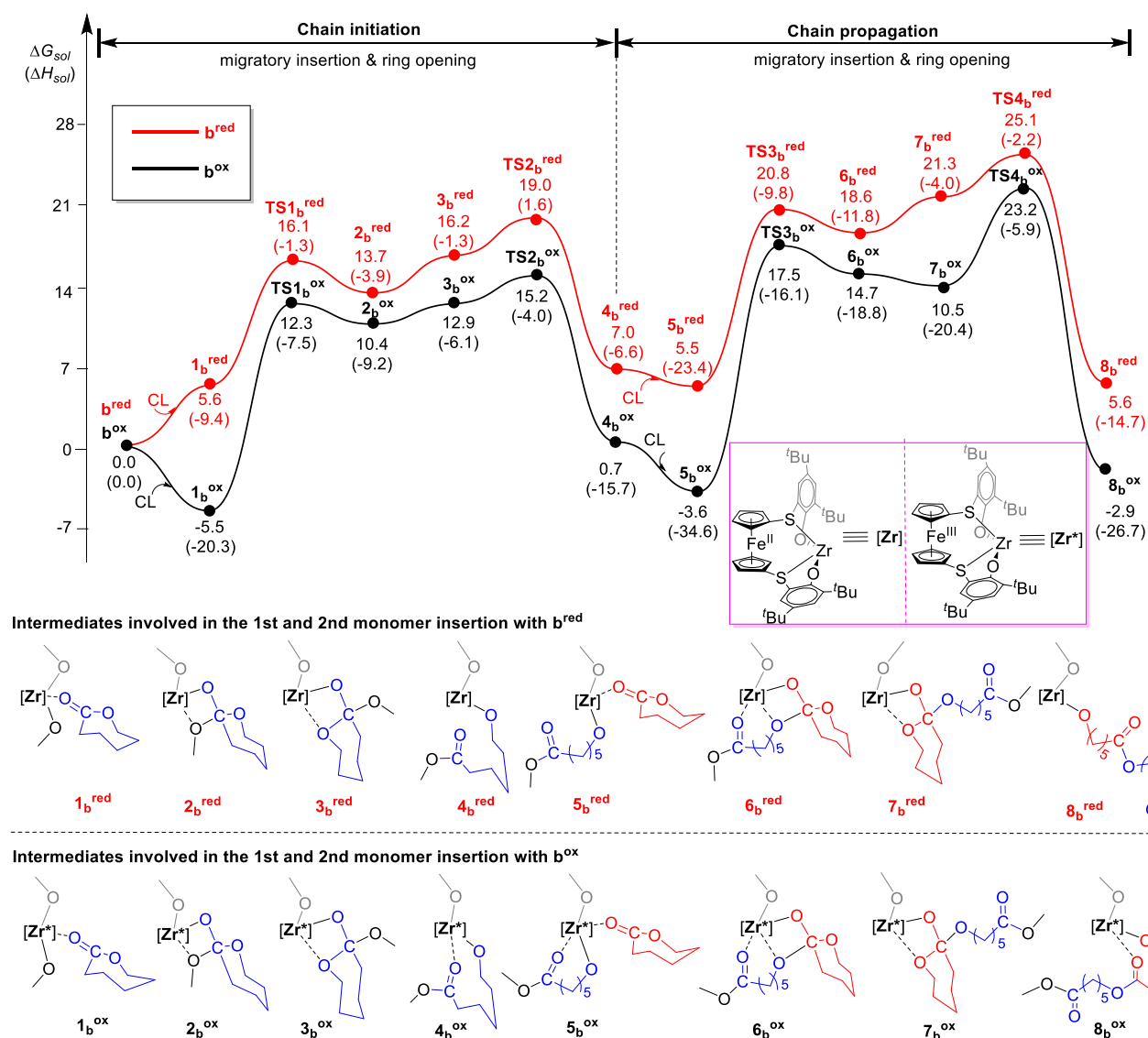


Fig. 6 Energy profiles of the chain initiation and propagation steps catalyzed by b^{ox} and b^{red}. The relative free energy and enthalpy values (in parentheses) are given in kcal mol⁻¹.

ARTICLE

To verify this hypothesis, the binding energies (ΔE_{bond}) between the metal complex and CL monomer in $\mathbf{1}_b^{\text{ox}}$ and $\mathbf{1}_b^{\text{red}}$ were calculated. As expected, the results show that the binding in $\mathbf{1}_b^{\text{ox}}$ ($\Delta E_{\text{bond}} = -19.9 \text{ kcal mol}^{-1}$) is stronger than that in $\mathbf{1}_b^{\text{red}}$ ($\Delta E_{\text{bond}} = -13.3 \text{ kcal mol}^{-1}$). The difference in the binding energy could also be explained by the charge and thus the Lewis acidity of the catalytic metal center. For example, the Mulliken charge of Zr in $\mathbf{1}_b^{\text{ox}}$ is more positive compared to that in $\mathbf{1}_b^{\text{red}}$ (1.60 vs 1.40), and the similar is true for $\mathbf{5}_b^{\text{ox}}$ and $\mathbf{5}_b^{\text{red}}$ (see also the detailed change in the catalytic metal center charge along with the reaction pathway shown in Fig. S7).

In comparison with the $\mathbf{a}^{\text{red}}/\mathbf{a}^{\text{ox}}$ system, the energy barriers for the \mathbf{b} -mediated reactions are lower (28.7 and 25.1 vs 32.7 and 38.2 kcal mol^{-1} , Figs 2 and 6), suggesting an overall higher activity of catalysts \mathbf{b} than \mathbf{a} . This is in line with the experimental findings that the CL conversion in the $\mathbf{b}^{\text{red}}/\mathbf{b}^{\text{ox}}$ system (50 °C) is higher than that in the $\mathbf{a}^{\text{red}}/\mathbf{a}^{\text{ox}}$ systems (100 °C).^{6a,f} This could be attributed to the stronger interaction between the active species and monomers in the $\mathbf{b}^{\text{red}}/\mathbf{b}^{\text{ox}}$ systems, a consequence of the stronger Lewis acidity of the catalytic metal center in $\mathbf{b}^{\text{red}}/\mathbf{b}^{\text{ox}}$, as suggested by its charge (1.44 in \mathbf{b}^{red} vs 1.14 in \mathbf{a}^{red} , 1.48 in \mathbf{b}^{ox} vs 1.28 in \mathbf{a}^{ox} , Fig. 1).

ROP of CL Catalyzed by $\mathbf{c}^{\text{ox}}/\mathbf{c}^{\text{red}}$

Compared with $\mathbf{b}^{\text{ox}}/\mathbf{b}^{\text{red}}$ system, the supporting ligand in $\mathbf{c}^{\text{ox}}/\mathbf{c}^{\text{red}}$ has an additional methylene unit linking sulphur and the phenyl group. This difference renders \mathbf{c} with a different redox switchable property.^{6a,f} That is, unlike \mathbf{b} , \mathbf{c}^{ox} was more active than \mathbf{c}^{red} toward CL polymerization.^{6f} This phenomenon stimulated us to study the $\mathbf{c}^{\text{ox}}/\mathbf{c}^{\text{red}}$ mediated CL ROP. As shown in Fig. 7, all of the stationary points involved in the \mathbf{c}^{ox} -mediated reaction pathway are more stable than those of the corresponding reduced species. The overall energy barriers are 26.2 kcal mol^{-1} ($\mathbf{TS4}_e^{\text{ox}}$) and 31.3 kcal mol^{-1} ($\mathbf{TS4}_e^{\text{red}}$) for the oxidized and reduced cases, respectively. This result is in line with the experimentally observed difference between the two states.^{6f} The distortion/interaction (Fig. S8) and geometric structure (Figs. S9 and S10) analyses show that the stronger interaction between the catalyst and the monomer moieties contribute to the higher stability of the oxidized species. This can be also attributed to the relatively stronger Lewis acidity of the catalytic metal center in the oxidized species (Fig. S11) that could be responsible for the switchable activity, similarly to the aforementioned systems $\mathbf{a}^{\text{red}}/\mathbf{a}^{\text{ox}}$ and $\mathbf{b}^{\text{red}}/\mathbf{b}^{\text{ox}}$.

The Wiberg bond indices (WBI) of the Zr–S and Zr–O (ancillary ligand) bonds in $\mathbf{b}^{\text{ox}}/\mathbf{b}^{\text{red}}$ are larger than those in $\mathbf{c}^{\text{red}}/\mathbf{c}^{\text{ox}}$ (Table S1), suggesting a stronger Zr–ligand binding. This could provide an explanation for the more positively charged Zr atom in \mathbf{b} than in \mathbf{c} (Fig. 1).

Effects of Metal Centre and Auxiliary Ligand

According to the discussion above, it is noteworthy that the Lewis acidity of the metal center and the chelation of the lactone carbonyl group play an important role in the redox-switchable activity of the group 4 metal complexes toward ROP of CL. In order to understand trends in these redox-switchable systems, analogous species with different catalytic metal centers and donors in the supporting ligand were modeled computationally. For example, replacing the catalytic metal Zr with Hf gives $\mathbf{d}^{\text{ox}}/\mathbf{d}^{\text{red}}$, and replacing the coordinating S atom by O and Se atoms, provides $\mathbf{e}^{\text{ox}}/\mathbf{e}^{\text{red}}$ and $\mathbf{f}^{\text{ox}}/\mathbf{f}^{\text{red}}$, respectively (Fig. 8). It was found that the Lewis acidity of the catalytic metal centers is different between the two states of the newly designed species except for \mathbf{e} , where both species show the same charge for zirconium (Fig. 8). Interestingly, species \mathbf{e} show the highest zirconium charge (1.61) of all the investigated species. The chain initiation and propagation of CL polymerization catalyzed by $\mathbf{d}^{\text{ox}}/\mathbf{d}^{\text{red}}$, $\mathbf{e}^{\text{ox}}/\mathbf{e}^{\text{red}}$, and $\mathbf{f}^{\text{ox}}/\mathbf{f}^{\text{red}}$ were also calculated and the relevant data are collected in Table 2. The corresponding data of $\mathbf{a}^{\text{ox}}/\mathbf{a}^{\text{red}}$, $\mathbf{b}^{\text{ox}}/\mathbf{b}^{\text{red}}$, and $\mathbf{c}^{\text{ox}}/\mathbf{c}^{\text{red}}$ systems are also included in this table for comparison. The results suggest that $\mathbf{d}^{\text{ox}}/\mathbf{d}^{\text{red}}$ and $\mathbf{f}^{\text{ox}}/\mathbf{f}^{\text{red}}$ have a similar catalytic performance, as suggested by the energy barriers (31.5 kcal mol^{-1} for both oxidized forms, 24.3 and 24.7 kcal mol^{-1} for the reduced forms, respectively). In view of the moderate energy barriers for the reduced forms, it seems that both \mathbf{d}^{red} and \mathbf{f}^{red} could achieve ROP of CL under ambient conditions. It is noteworthy that, in comparison with $\mathbf{b}^{\text{ox}}/\mathbf{b}^{\text{red}}$, $\mathbf{d}^{\text{ox}}/\mathbf{d}^{\text{red}}$ (or $\mathbf{f}^{\text{ox}}/\mathbf{f}^{\text{red}}$) may have a larger activity difference between the two states for the ROP of CL because of their larger energy barrier difference (Table 2). In the case of $\mathbf{e}^{\text{ox}}/\mathbf{e}^{\text{red}}$, however, the energy barriers are almost same (27.0 and 27.4 kcal mol^{-1}) for the two oxidation states. This suggests that \mathbf{e} may have no redox-switchable character in the ROP of CL. These results indicate that a careful regulation of the catalytic metal center and the ancillary ligand could provide a different redox-switchable activity toward the ROP of CL.

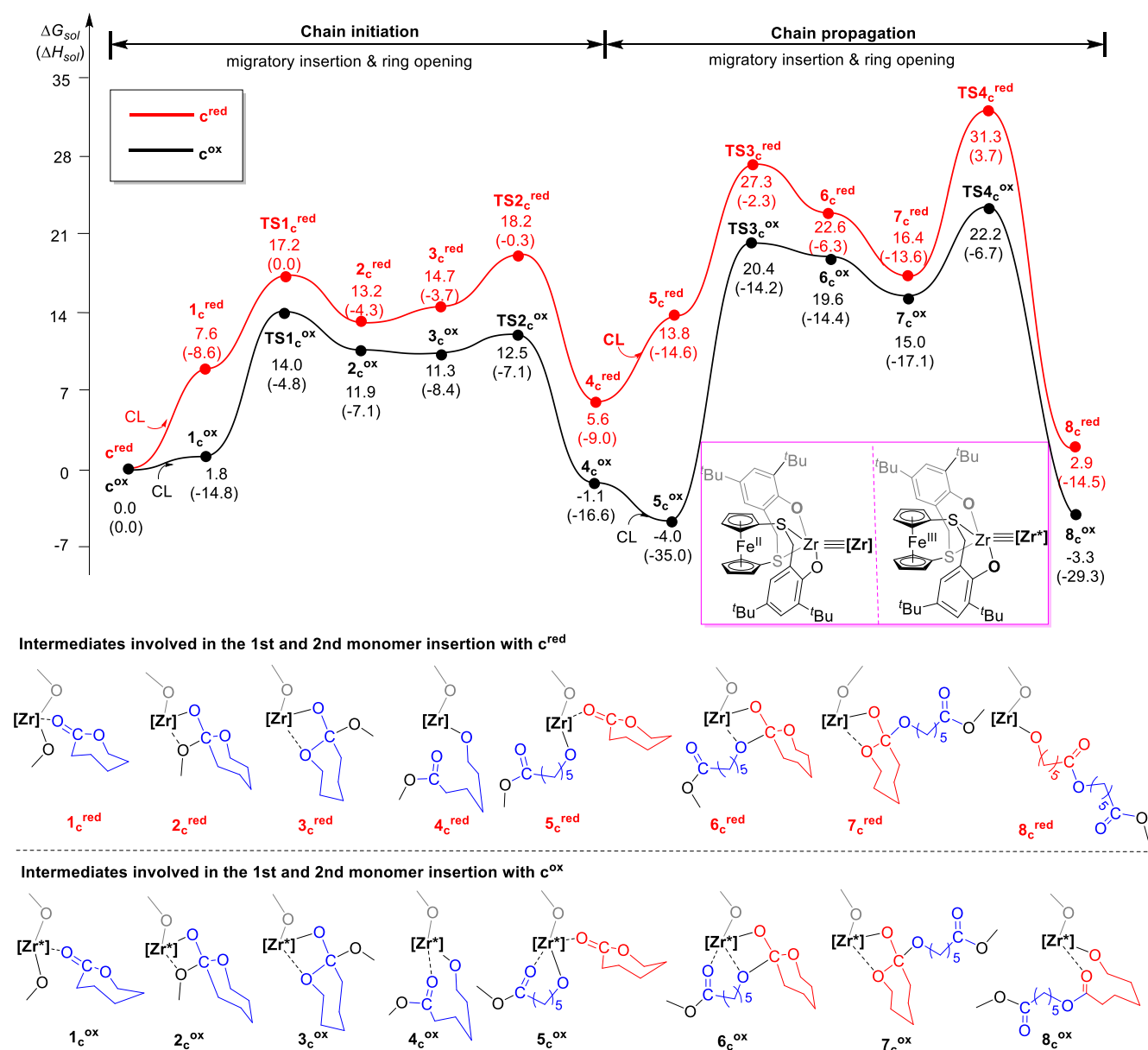


Fig. 7 Energy profiles of the chain initiation and propagation mediated by c^{ox} and c^{red} . The relative free energies and enthalpy values (in parentheses) are given in kcal mol⁻¹.

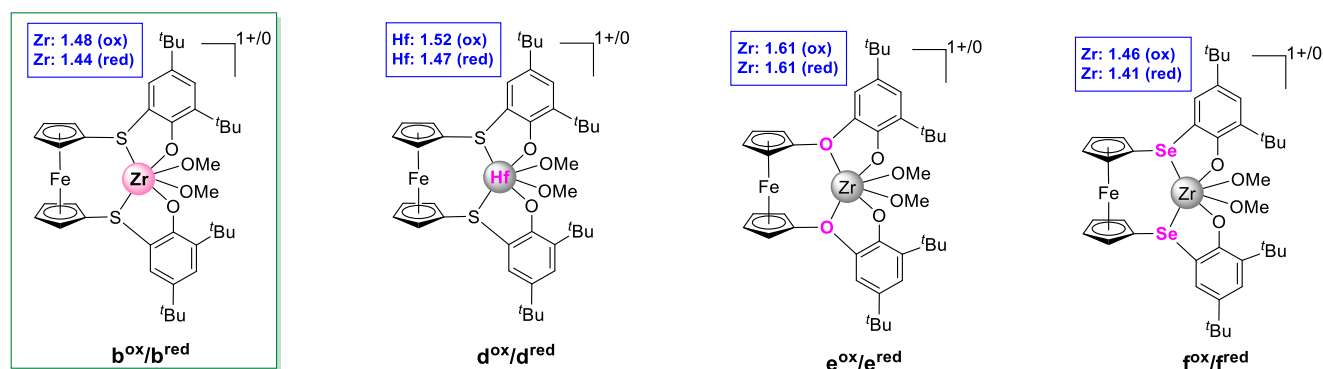


Fig. 8 Designed group 4 metal alkoxide analogues based on the $b^{\text{ox}}/b^{\text{red}}$. Mulliken charges on metal atoms are given in blue, respectively. The “red” and “ox” in parentheses refer to the reduced and oxidized forms, respectively.

ARTICLE

Table 2. The computed free energies (kcal mol⁻¹) in solution for the chain initiation and propagation of CL polymerization catalyzed by **a-f**.

species	1 ^a	TS1	TS2	5	TS3	TS4	ΔG^\ddagger ^b
a ^{ox}	1.6	17.8	23.6	13.7	32.7	25.7	32.7
a ^{red}	10.7	23.5	29.8	11.7	27.1	38.2	38.2
b ^{ox}	-5.5	12.3	15.2	-3.6	17.5	23.2	28.7
b ^{red}	5.6	16.1	19.0	5.5	20.8	25.1	25.1
c ^{ox}	1.8	14.0	12.5	-4.0	20.4	22.2	26.2
c ^{red}	7.6	17.2	18.2	5.6	27.3	31.3	31.3
d ^{ox}	-8.4	10.1	12.4	-2.6	13.4	23.1	31.5
d ^{red}	2.3	14.4	17.6	5.3	19.9	24.3	24.3
e ^{ox}	-8.5	10.0	11.7	-4.9	10.9	18.5	27.0
e ^{red}	6.0	13.3	14.3	7.8	20.4	27.4	27.4
f ^{ox}	-3.3	13.2	16.4	0.5	20.9	28.2	31.5
f ^{red}	4.8	15.3	18.9	4.7	20.7	24.7	24.7

^a**1** and **5** denote the coordination complexes of the first and the second monomer, respectively.^b ΔG^\ddagger represents the overall free energy barrier for CL polymerization.

Conclusions

The redox-switchable ring-opening polymerization mechanism of ϵ -caprolactone catalyzed by three group 4 metal complexes bearing [OSSO]-type bis(phenolato) ferrocene ligands (i.e., **a**^{ox}/**a**^{red}, **b**^{ox}/**b**^{red}, and **c**^{ox}/**c**^{red}) was investigated by DFT calculations. Having achieved an agreement between calculation and experiment, it was found that the higher activity of the oxidized forms **a**^{ox} and **c**^{ox} compared to that of their corresponding reduced forms stems from the higher Lewis acidity of the catalytic metal center in the oxidized species. In contrast, the lower activity of the oxidized species **b**^{ox} compared to that of **b**^{red} is due to an increased stability of the intermediate following the monomer coordination that results in a high energy barrier. The current results also indicate that the stronger Lewis acidity of the catalytic metal center generally increases the activity of the catalyst. However, it could also increase the energy barrier of a reaction when the Lewis acidity of metal center is strong enough to overstabilize the coordination complex. It is noteworthy that such a redox-induced Lewis acidity variation and thus switchable activity is different from the case of redox-switchable polymerization of trimethylene carbonate catalyzed by ferrocene-based indium complexes, where the oxidation of the ferrocene unit altered the coordination ability of the catalytic metal center rather than its Lewis acidity. In the series of [OSSO]-type bis(phenolato) ferrocene-based group 4 metal complexes, our computational modelling indicates that a Hf analogue may possess better redox-switchable property for the ROP of CL compared to its corresponding Zr complex. Furthermore, the redox-switchable activity of the Zr complexes with different bridging-heteroatoms in their ancillary ligands follows the order of O < S

< Se. These findings are expected to provide useful information on developing new redox-switchable polymerization catalysts for the synthesis of biodegradable polymers from biomass-derived monomers.

Conflicts of interest

There are no conflicts to declare.

Acknowledgements

This work was supported by the NSFC (21674014, U1862115). Y.L. and G.L. thank the Fundamental Research Funds for the Central Universities (DUT18GJ201, DUT18RC(3)002). PLD thanks the National Science Foundation for grant CHE-1809116. The authors also thank RICC (RIKEN Integrated Cluster of Clusters) and the Network and Information Center of Dalian University of Technology for part of computational resources.

Notes and references

- (a) N. Siddiqui, S. Asawa, B. Birru, R. Baadhe and S. Rao, *Mol. Biotechnol.*, 2018, **60**, 506; (b) E. Malikmammadov, T. E. Tanir, A. Kiziltay, V. Hasirci and N. Hasirci, *J. Biomater. Sci., Polym. Ed.* 2018, **29**, 863; (c) R. Auras, L. -T. Lim, S. E. M. Selke and H. Tsuji, *Poly(Lactic Acid): Synthesis, Structures, Properties, Processing, and Applications*, 2010, Wiley & Sons, Inc.
- (a) K. M. Osten and P. Mehrkhodavandi, *Acc. Chem. Res.* 2017, **50**, 2861; (b) T. Fuoco and D. Pappalardo, *Catalysts* 2017, **7**, 64; (c) S. Dagorne, M. Normand, E. Kirillov and J. -F. Carpentier, *Coord. Chem. Rev.* 2013, **257**, 1869; (d) S. Dutta, W. -C. Hung, B. -H. Huang and C. -C. Lin, *Adv. Polym. Sci.* 2012,

- 245**, 219; (e) M. Labet and W. Thielemans, *Chem. Soc. Rev.* 2009, **38**, 3484; (f) J. Wu, T. Yu, C. Chen and C. Lin, *Coord. Chem. Rev.* 2006, **250**, 602; (g) O. Dechy-Cabaret, B. Martin-Vaca, D. Bourissou, *Chem. Rev.* 2004, **104**, 6147; (h) B. J. O'Keefe, M. A. Hillmyer and W. B. Tolman, *J. Chem. Soc., Dalton Trans.* 2001, 2215.
- 3 (a) J. Wei and P. L. Diaconescu, *Acc. Chem. Res.* 2019, **52**, 415; (b) C. Chen, *ACS Catal.* 2018, **8**, 5506; (c) A. J. Teator, D. N. Lastovickova and C. W. Bielawski, *Chem. Rev.* 2016, **116**, 1969; (d) S. M. Guillaume, E. Kirillov, Y. Sarazin and J. -F. Carpentier, *Chem. -Eur. J.* 2015, **21**, 7988.
 - 4 C. K. A. Gregson, V. C. Gibson, N. J. Long, E. L. Marshall, P. J. Oxford and A. J. P. White, *J. Am. Chem. Soc.* 2006, **128**, 7410.
 - 5 (a) K. R. Delle Chiaie, A. B. Biernesser, M. A. Ortuno, B. Dereli, D. A. Iovan, M. J. T. Wilding, B. Li, C. J. Cramer and J. A. Byers, *Dalton Trans.* 2017, **46**, 12971. (b) A. B. Biernesser, K. R. Delle Chiaie, J. B. Curley and J. A. Byers, *Angew. Chem., Int. Ed.* 2016, **55**, 5251; (c) Y. Y. Fang, W. J. Gong, X. J. Shang, H. X. Li, J. Gao and J. P. Lang, *Dalton Trans.* 2014, **43**, 8282; (d) A. B. Biernesser, B. Li and J. A. Byers, *J. Am. Chem. Soc.* 2013, **135**, 16553; (e) A. Sauer, J. -C. Buffet, T. P. Spaniol, H. Nagae, K. Mashima and J. Okuda, *ChemCatChem* 2013, **5**, 1088; (f) E. M. Broderick, N. Guo, T. Wu, C. S. Vogel, C. Xu, J. Sutter, J. T. Miller, K. Meyer, T. Cantat and P. L. Diaconescu, *Chem. Commun.* 2011, **47**, 9897.
 - 6 (a) M. Y. Lowe, S. Shu, S. M. Quan and P. L. Diaconescu, *Inorg. Chem. Front.* 2017, **4**, 1798; (b) J. Wei, M. N. Riffel and P. L. Diaconescu, *Macromolecules* 2017, **50**, 1847; (c) S. M. Quan, J. Wei and P. L. Diaconescu, *Organometallics* 2017, **36**, 4451; (d) S. M. Quan, X. Wang, R. Zhang and P. L. Diaconescu, *Macromolecules* 2016, **49**, 6768; (e) L. A. Brown, J. L. Rhinehart and B. K. Long, *ACS Catal.* 2015, **5**, 6057. (f) X. Wang, A. Thevenon, J. L. Brosmer, I. Yu, S. I. Khan, P. Mehrkhodavandi and P. L. Diaconescu, *J. Am. Chem. Soc.* 2014, **136**, 11264; (g) A. Lai, Z. C. Hern and P. L. Diaconescu, *ChemCatChem* DOI: 10.1002/cctc.201900747.
 - 7 M. A. Ortuno, B. Dereli, K. R. D. Chiaie, A. B. Biernesser, M. Qi and J. A. Byers, C. J. Cramer, *Inorg. Chem.* 2018, **57**, 2064.
 - 8 (a) G. Zhou, X. Kang, X. Wang, Z. Hou and Y. Luo, *Organometallics* 2018, **37**, 551; (b) C. Wang, G. Luo, M. Nishiura, G. Song, A. Yamamoto, Y. Luo and Z. Hou, *Sci. Adv.* 2017, **3**, e1701011; (c) X. Hu, X. Kang, G. Zhou, X. Wang, Z. Hou and Y. Luo, *Chin. J. Chem.* 2017, **35**, 723; (d) X. Kang, G. Zhou, X. Wang, J. Qu, Z. Hou and Y. Luo, *Organometallics* 2016, **35**, 913; (e) G. Luo, Y. Luo and Z. Hou, J. Qu, *Organometallics* 2016, **35**, 778; (f) L. Luo, X. Kang, G. Zhou, S. Chen, G. Luo, J. Qu and Y. Luo, *Int. J. Quantum Chem.* 2016, **116**, 1274; (g) X. Wang, F. Lin, J. Qu, Z. Hou and Y. Luo, *Organometallics* 2016, **35**, 3205; (h) X. Kang, A. Yamamoto, M. Nishiura, Y. Luo and Z. Hou, *Organometallics* 2015, **34**, 5540; (i) X. Kang, Y. Luo, G. Zhou, X. Wang, X. Yu, Z. Hou and J. Qu, *Macromolecules* 2014, **47**, 4596; (j) X. Kang, Y. Song, Y. Luo, G. Li, Z. Hou and J. Qu, *Macromolecules* 2012, **45**, 640; (k) Y. Luo, Y. Luo, J. Qu and Z. Hou, *Organometallics* 2011, **30**, 2908.
 - 9 X. Xu, G. Luo, A. Mehmood, Y. Zhao, G. Zhou, Z. Hou and Y. Luo, *Organometallics* 2018, **37**, 4599.
 - 10 (a) J. P. Perdew, K. Burke and Y. Wang, *Phys. Rev. B* 1996, **54**, 16533; (b) A. D. Becke, *J. Chem. Phys.* 1993, **98**, 5648; (c) J. P. Perdew and Y. Wang, *Phys. Rev. B: Condens. Matter Mater. Phys.* 1992, **45**, 13244.
 - 11 S. Grimme, J. Antony, S. Ehrlich and H. A. Krieg, *J. Chem. Phys.* 2010, **132**, 154104.
 - 12 (a) P. C. Hariharan and J. A. Pople, *Theor. Chim. Acta* 1973, **28**, 213; (b) W. J. Hehre, R. Ditchfield and J. A. Pople, *J. Chem. Phys.* 1972, **56**, 2257.
 - 13 (a) J. M. L. Martin and A. Sundermann, *J. Chem. Phys.* 2001, **114**, 3408; (b) M. Dolg, H. Stoll and H. Preuss, *J. Chem. Phys.* 1989, **90**, 1730.
 - 14 Y. Zhao and D. G. Truhlar, *Theor. Chem. Acc.* 2008, **120**, 215.
 - 15 (a) M. Cossi, N. Rega, G. Scalmani and V. Barone, *J. Comput. Chem.* 2003, **24**, 669; (b) V. Barone and M. Cossi, *J. Phys. Chem. A* 1998, **102**, 1995.
 - 16 M. J. Frisch, G. W. Trucks, H. B. Schlegel, G. E. Scuseria, M. A. Robb, J. R. Cheeseman, G. Scalmani, V. Barone, B. Mennucci, G. A. Petersson, H. Nakatsuji, M. Caricato, X. Li, H. P. Hratchian, A. F. Izmaylov, J. Bloino, G. Zheng, J. L. Sonnenberg, M. Hada, M. Ehara, K. Toyota, R. Fukuda, J. Hasegawa, M. Ishida, T. Nakajima, Y. Honda, O. Kitao, H. Nakai, T. Vreven, J. A. Montgomery, J. E. Peralta, F. Ogliaro, M. Bearpark, J. J. Heyd, E. Brothers, K. N. Kudin, V. N. Staroverov, T. Keith, R. Kobayashi, J. Normand, K. Raghavachari, A. Rendell, J. C. Burant, S. S. Iyengar, J. Tomasi, M. Cossi, N. Rega, J. M. Millam, M. Klene, J. E. Knox, J. B. Cross, V. Bakken, C. Adamo, J. Jaramillo, R. Gomperts, R. E. Stratmann, O. Yazyev, A. J. Austin, R. Cammi, C. Pomelli, J. W. Ochterski, R. L. Martin, K. Morokuma, V. G. Zakrzewski, G. A. Voth, P. Salvador, J. J. Dannenberg, S. Dapprich, A. D. Daniels, O. Farkas, J. B. Foresman, J. V. Ortiz, J. Cioslowski and D. J. Fox, *Gaussian 16, Revision B.01*, Gaussian, Inc., Wallingford CT, 2016.
 - 17 Legault, C. Y., Cylview, version 1.0 b. *Université de Sherbrooke* 2009, <http://www.cylview.org/>.
 - 18 M. Abubekkerov, V. Vlcek, J. Wei, M. E. Miehlich, S. M. Quan, K. Meyer, D. Neuhauser and P. L. Diaconescu, *iScience* 2018, **7**, 120.
 - 19 Y. Shen, S. M. Shepard, C. J. Reed and P. L. Diaconescu, *Chem. Commun.*, 2019, **55**, 5587.
 - 20 C. M. Thomas, *Chem. Soc. Rev.* 2010, **39**, 165; (b) A. Arbaoui and C. Redshaw, *Polym. Chem.* 2010, **1**, 801.
 - 21 (a) K. Kitaura and K. Morokuma, *Int. J. Quantum Chem.* 1976, **10**, 325; (b) F. M. Bickelhaupt and K. N. Houk, *Angew. Chem., Int. Ed.* 2017, **56**, 10070; (c) F. Liu, Y. Liang, and K. N. Houk, *Acc. Chem. Res.* 2017, **50**, 2297; (d) I. Fernández and F. M. Bickelhaupt, *Chem. Soc. Rev.* 2014, **43**, 4953.

